Published in final edited form as:
J Neurosci. 2011 March 30; 31(13): 4886–4895. doi:10.1523/JNEUROSCI.5122-10.2011.

Probing the functional equivalence of otoferlin and synaptotagmin 1 in exocytosis

Ellen Reisinger[1], **Chris Bresee**[2], **Jakob Neef**[3,+], **Ramya Nair**[4,+], **Kirsten Reuter**[1,+], **Anna Bulankina**[3], **Régis Nouvian**[3,5], **Manuel Koch**[3], **Johanna Bückers**[6], **Lars Kastrup**[6], **Isabelle Roux**[7,8], **Christine Petit**[7], **Stefan W. Hell**[6,9], **Nils Brose**[9,10], **Jeong-Seop Rhee**[4], **Sebastian Kügler**[9,11,*], **John Brigande**[2,*], and **Tobias Moser**[3,9,*]

[1]Molecular Biology of Cochlear Neurotransmission, Dept. of Otolaryngology, University Medical Center Goettingen, 37099 Göttingen, Germany

[2]Oregon Hearing Research Center, Oregon Health & Science University, Portland, OR 97239, USA

[3]InnerEarLab, Dept. of Otolaryngology, University Medical Center Goettingen, 37099 Göttingen, Germany

[4]Neurophysiology Group, Department of Molecular Neurobiology, Max Planck Institute of Experimental Medicine, 37075 Göttingen, Germany

[6]Department of NanoBiophotonics, Max Planck Institute for Biophysical Chemistry, 37077 Göttingen, Germany

[7]Inserm UMRS587, Unite de Genetique des Deficits Sensoriels, College de France, Institut Pasteur, 75015 Paris, France

[9]Center for Molecular Physiology of the Brain, University of Göttingen, Germany

[10]Department of Molecular Neurobiology, Max Planck Institute of Experimental Medicine, Göttingen, Germany

[11]Department of Neurology, University Medical Center Goettingen, 37099 Göttingen, Germany

Abstract

Cochlear inner hair cells (IHCs) use Ca^{2+}-dependent exocytosis of glutamate to signal sound information. Otoferlin, a C_2-domain protein essential for IHC exocytosis and hearing, may serve as a Ca^{2+} sensor in vesicle fusion in IHCs that seem to lack the classical neuronal Ca^{2+} sensors synaptotagmin 1 (Syt1) and 2. Support for the Ca^{2+} sensor of fusion hypothesis for otoferlin function comes from biochemical experiments, but additional roles in late exocytosis upstream of fusion have been indicated by physiological studies. Here, we tested the functional equivalence of otoferlin and Syt1 in three neurosecretory model systems: auditory IHCs, adrenal chromaffin cells and hippocampal neurons. Long-term and short-term ectopic expression of Syt1 in IHCs of

[*]**Correspondence to:** Tobias Moser, InnerEarLab, Department of Otolaryngology, Göttingen University Medical School, 37099 Göttingen, Germany, Phone: +49-551-398968, Fax: +49-551-3912950, tmoser@gwdg.de, or John V. Brigande, Oregon Hearing Research Center, Oregon Health and Science University 3181 SW Sam Jackson Park Rd/NRC04, Portland, OR 97239 USA, Phone: (503) 494-2933, Fax: (503) 494-5656, brigande@ohsu.edu, or Sebastian Kügler, Department of Neurology, University of Göttingen Medical Center, 37099 Göttingen, Germany, Phone: +49-551-398351, Fax: +49-551-3914476, sebastian.kuegler@med.uni-goettingen.de.

[5]present address: Inserm U1051, Institut des Neurosciences de Montpellier, 34091 Montpellier, France

[8]present address: The Johns Hopkins School of Medicine, Department of Otolaryngology-Head and Neck Surgery, Baltimore, MD 21205, USA

[+]equal contribution

Conflict of interest: The authors state no conflict of interest

Otof$^{-/-}$ mice by viral gene transfer in the embryonic inner ear and organotypic culture failed to rescue their Ca^{2+} influx-triggered exocytosis. On the other hand, virally mediated overexpression of otoferlin did not restore phasic exocytosis in Syt1-deficient chromaffin cells or neurons, but enhanced asynchronous release in the latter. We further tested exocytosis in *Otof*$^{-/-}$ hippocampal neurons and in *Syt1*$^{-/-}$ IHCs, but found no deficits in vesicle fusion. Expression analysis of different synaptotagmin isoforms indicated that Syt1 and Syt2 are absent from mature IHCs. Our data argue against a simple functional equivalence of the two C_2 domain proteins in exocytosis of IHC ribbon synapses, chromaffin cells and hippocampal synapses.

Keywords

cochlea; hair cell; hippocampal neuron; synapse; chromaffin cell; *in utero* gene transfer

Introduction

Hearing relies on temporally precise and reliable Ca^{2+} influx-driven exocytosis of synaptic vesicles at the ribbon-type active zones of hair cells. The multi-C_2 domain protein otoferlin was shown to be essential in a late step of exocytosis, as absence of this protein nearly abolishes vesicle fusion despite the presence of docked vesicles (Roux et al., 2006). C_2 domains mediate Ca^{2+}-dependent and -independent phospholipid binding and are involved in cellular signaling, synaptic vesicle exocytosis and plasma membrane repair (reviewed in Rizo and Sudhof, 1998; Cho and Stahelin, 2005; McNeil and Kirchhausen, 2005; Martens and McMahon, 2008). The presence of several C_2 domains in otoferlin, some of which bind Ca^{2+}, led to the hypothesis that otoferlin might be a Ca^{2+} sensor for fusion in IHC synapses (Roux et al., 2006; Ramakrishnan et al., 2009; Johnson and Chapman, 2010). This notion was supported by the finding that other potential Ca^{2+} sensors like Syt1, 2 and 3 are missing from the hair cell synapse (Safieddine and Wenthold, 1999), a finding that is currently under debate (Beurg et al., 2010; Johnson et al., 2010). Otoferlin co-precipitates with the SNARE proteins SNAP-25 and syntaxin 1 (Roux et al., 2006), and individual otoferlin C_2 domains stimulate the fusion of liposomes loaded with reconstituted SNAREs in presence of Ca^{2+} (Johnson and Chapman, 2010). One obvious test of the Ca^{2+} sensor hypothesis of otoferlin function would be to probe the functional equivalence of both proteins in supporting vesicle fusion in otoferlin- and Syt1-dependent neurosecretory preparations.

Otoferlin and Syt1 seem to serve multiple functions in regulating vesicle cycling. Studying a missense mutation of *Otof* originating from an ENU mutagenesis screen (Schwander et al., 2007), we recently implicated otoferlin in efficient vesicle replenishment at the inner hair cell active zone (Pangrsic et al., 2010). Given the multiple protein interactions of otoferlin (Heidrych et al., 2009; Roux et al., 2009) it might even serve further, undiscovered functions at the presynaptic active zone. Several functions have also been assigned to Syt1: besides its role as Ca^{2+} sensor for vesicle fusion, it has been shown to function in vesicle replenishment (docking of large dense core vesicles: Chieregatti et al., 2002; de Wit et al., 2009), in positional priming of synaptic vesicles (Young and Neher, 2009), and in endocytosis (Nicholson-Tomishima and Ryan, 2004).

While a more general comparison of the functional properties of otoferlin to the well characterized Syt1 continues to be of interest, in this study we focused on the question whether otoferlin and Syt1 can functionally substitute for one another to preserve synchronous vesicle fusion. We tested for such cross-rescue in Syt1-dependent and in otoferlin-dependent neurosecretory preparations. Our results demonstrate that neither ectopic expression of otoferlin in Syt1-deficient chromaffin cells and hippocampal neurons nor ectopic expression of Syt1 in otoferlin-deficient cochlear IHCs restores synchronous

exocytosis, arguing against a simple functional equivalence of these two proteins. Furthermore, otoferlin deletion did not affect transmitter release at hippocampal synapses and vesicle fusion appeared unchanged in Syt1 deficient IHCs.

Materials and Methods

Mouse mutagenesis

To generate *Otof*$^{-/-}$ mice, a targeting vector was constructed in which exons 14 and 15 of the wild-type *Otof* gene were replaced by a loxP flanked Neomycin selection cassette by subcloning into the NdeI and NsiI restriction sites located in the respective intron regions. The targeting construct consisted of 2.7 kb and 5.3 kb long linkers for homologous recombination upstream and downstream of the loxP flanked Neomycin cassette. A thymidine kinase cassette for negative selection was added after the 5.3 kb long arm. This targeting construct was electroporated into 129ola embryonic stem cells, and cell colonies were picked after selection with G418 and ganciclovir. Homologous recombination was tested by Southern Blot analysis after BclI digest using a BclI site upstream exon 11 and a newly introduced BclI site next to NdeI. From 96 cell clones analyzed, 6 were found to show the Southern blot pattern expected for homologous recombination (7.5 kb band). Two of these clones were injected into mouse blastocysts, which both led to germ line transmission in male chimeric mice. Heterozygous offspring from the chimeras were bred with a cre-recombinase expressing mouse line to excise the neomycin cassette. Excision of exons 14 and 15 leads to a frameshift and premature stop during translation of the Otof mRNA. In immunostainings of the cochlea, otoferlin protein was not detectable in *Otof* $^{-/-}$ mice with antibodies targeting N- or C- terminus of the protein (see Pangrsic et al., 2010).

Virus transduction of IHCs

Adeno-assosicated virus (AAV) containing inverted terminal repeats of serotype 2 and capsid proteins of serotypes 1 and 2 (AAV-1/2) was prepared as described (Kugler et al., 2007). For *in vitro* transduction, coverslips were coated with Celltak (BD Biosciences) and air-dried. Organs of Corti of postnatal day 0 (p0) mice (*Syt1*$^{-/-}$ and control littermates) or p8–9 mice (*Otof*$^{-/-}$ and wild-type controls) were dissected in sterile balanced HEPES-buffered Hanks' solution containing 250 ng/ml fungizone and 10 μg/ml penicillin. Dissected organs of Corti were placed in DMEM-F12 with 5% FBS and attached to the coverslips by gentle pressure. After one day in vitro (DIV), organotypic cultures were washed once in PBS, and 300 μl DMEM-F12 (without FBS), containing 8×10^8 particles of AAV-1/2, were applied. After 24 h, 300 μl of DMEM-F12 with 5% FBS were added to the cultures, and 1–2 days later, the medium was replaced with 1 ml DMEM-F12 with 5% FBS.

For *in vivo* transduction, viral inoculum (~250 nl, 4×10^8 particles/μl) was microinjected through the uterus into the mouse otocyst at embryonic day 11.5 to 12.5 as previously described (Gubbels et al., 2008; Brigande et al., 2009). Only the left otocyst of each embryo was injected and the uninjected contralateral ear served as an internal control.

Immunohistochemistry in organs of Corti, confocal microscopy and image analysis

For cochlear cryosections, temporal bones were fixed for 1h in 4% formaldehyde, decalcified (only at p19) for 48 h in 0.12 mM EDTA in PBS, incubated in 25% sucrose over night at 4°C and embedded in TissueTek (Shandon Cryomatrix, Thermo Scientific, UK). 16 μm cryosections or whole mount organs of Corti were immunostained as described (Khimich et al., 2005) using the following antibodies: monoclonal anti-otoferlin, dilution 1:500, Abcam, Cambrigde, UK; rabbit anti-VGlut3, 1:500; monoclonal anti-Syt1 (clone 41.1), 1:1000; rabbit or monoclonal anti-calbindin (1:2000), all from Synaptic Systems (SYSY), Göttingen, Germany; mouse monoclonal znp-1 (anti-Syt2) 1:1000 (Zebrafish

International Resource Center, Eugene, Oregon, USA) and secondary AlexaFluor488- and AlexaFluor568-labeled antibodies (Invitrogen, 1:200). Confocal images were acquired using a laser scanning confocal microscope (Leica TCS SP2 or SP5, Leica MicrosystemsCMS GmbH, Mannheim, Germany) with 488 nm (Ar) and 561 nm (He-Ne) lasers for excitation and 63x oil immersion objectives. Optical sections were acquired at steps of 0.7 μm and z-stacks were maximum-intensity-projected in ImageJ.

High resolution STED microscopy

Immunostaining of whole mount apical organ of corti turns was performed as for confocal microscopy with some variations. Excess primary antibody was removed by washing 10 min in 20 mM phosphate buffer, 0.3% Triton-X-100 and 0.45 M NaCl followed by three, 10 min washes in 2.5% goat serum in PBS. KK114-coupled sheep anti-mouse and Atto594-coupled goat antirabbit antibodies were applied 1:100 in 2.5% goat serum in PBS for 1h at room temperature. Organs of Corti were washed 3× 30–40 min in 10% goat serum in PBS and embedded in 2'2 Thiodiethanol as described (Staudt et al., 2007). Imaging was performed at 1 ms dwell-time (accomodating 1000 laser pulses) with ~ 0.5 μW excitation at wavelengths 570 nm and 650 nm and with ~ 1.5 mW STED power at wavelengths 720 nm and 755 nm in the objective's aperture. Fluorescence signals were detected at 620 nm and 670 nm, respectively. Images were background subtracted as estimated in a region of interest nearby the IHC and deconvoluted using the Richardson-Lucy algorithm with 25 iterations and a regularization parameter of 10^{-10}.

Auditory brainstem responses (ABR) and distortion product otoacoustic emissions (DPOAE)

Two separate sets of ABR data were recorded in Portland and Göttingen using slightly different equipment. In both cases, mice were anesthetized intraperitoneally with a ketamine/xylazine solution in 0.9% saline, needle electrodes were placed in the skin of vertex and subaurically and hearing threshold was determined with 10 dB precision as the lowest stimulus intensity that evoked a reproducible response waveform in both traces by visual inspection.

For data set 1 (Portland) a speaker was placed in the ear canal and a sequential stimulus consisting of pure tones of 4 to 32 kHz was executed, with each tone burst presented at 10 different intensities for 2 ms each. ABRs were recorded as 12 ms acquisitions. Data set 2 (Göttingen) was recorded as described in (Neef et al., 2009). In brief, tone bursts (4 to 32 kHz, 10 ms plateau, 1 ms $\cos^2$ rise/fall) or clicks of 0.03 ms were generated using Tucker-Davis-Technology (TDT, Ft. Lauderdale) hardware presented at 20 Hz in the free field ipsilaterally using a JBL 2402 speaker (JBL GmbH & Co., Neuhofen, Germany). The difference potential between vertex and mastoid subdermal needles was amplified (5e4-times), filtered (low pass: 4 kHz, high pass: 100 Hz) and sampled at a rate of 50 kHz for 20 ms, 2×2000 times to obtain two mean ABRs for each sound intensity. For ABR comparisons of injected and non-injected ears of wild-type mice the other ear was occluded with electrode gel and measured the other day in random order (gel was gone by then). For DPOAEs, a 24-bit sound card and the ED1/EC1 speaker system (TDT) were used to generate two primary tones (ratio f2/f1: 1.2). Primary tones were coupled into the ear canal by a custom-made probe containing an MKE-2 microphone (Sennheiser, Hannover, Germany) and adjusted to an intensity of 60 dB sound pressure level at the position of the ear drum as mimicked in a mouse ear coupler. The microphone signal was amplified (DMP3, MIDIMAN) and analyzed by fast Fourier transformation.

Patch-clamp of IHCs

All cell physiology experiments (IHCs, chromaffin cells and neurons) were performed at room temperature (20–25°C). IHCs from cultured organs of Corti from neonatal mice (see below) or from acute explants of the apical coil of the organ of Corti from 4-week-old mice were whole-cell patch-clamped essentially as described (Moser and Beutner, 2000). The pipette solution contained (in mM): 130 Cs-gluconate, 10 tetraethylammonium-Cl (TEA-Cl), 10 4-aminopyridine (4-AP), 10 Cs-HEPES, 1 $MgCl_2$, and amphotericin B (300 μg/ml, Calbiochem, La Jolla, CA, for perforated patch) or 2 mM Mg-ATP and 0.3 mM Na-GTP (for ruptured patch). The extracellular solution contained (in mM): 107 NaCl, 35 TEA-Cl, 10 HEPES, 5 4-AP, 2.8 KCl, 2 $CaCl_2$, 1 $MgCl_2$, 1 $CsCl_2$ and 11.2 glucose for acutely explanted organs of Corti (for cultured OCs: 105 NaCl, 10 $CaCl_2$ [to enhance the low Ca^{2+} currents (I_{Ca}) in cultured IHCs] and 100 nM apamin), 290–310 mOsmol/l, pH: 7.2. EPC-9 amplifiers (HEKA-electronics, Lambrecht, Germany) controlled by "Pulse" software (HEKA) were used for measurements. Currents were low-pass filtered at 2 or 4 kHz, sampled at 10 kHz and P/10 leak corrected. IHCs were discarded when leak currents exceeded −50 pA at −84 mV. Capacitance measurements were performed as described (Neef et al., 2009) using the Lindau-Neher technique implemented as the "sine+dc" mode of the "software lock-in" extension of PULSE software. A 1 kHz, 70 mV peak-to-peak sinusoid stimulus was applied about a DC holding potential of −84 mV.

Single Cell Real Time PCR

Real time PCR for the detection of 14 Syt isoforms was performed as described (Kerr et al., 2008). Briefly, a patch pipette, filled as described above for ruptured patch, was approached with positive pressure towards an individual rat IHC and used to aspirate its cytoplasm. The contents of the pipette were expelled into a solution for reverse transcription of mRNA. The cDNA was ethanol precipitated and amplicons were pre-amplified with 15 cycles of a multiplex PCR prior to the real-time-PCR. Samples from each cell were split to perform TaqMan real-time-PCR for each Syt isoform in a separate reaction tube (sequences of oligos and TaqMan probes as in (Kerr et al., 2008). For negative controls, bath solution in close proximity to IHCs was aspirated into patch pipettes before and after IHC-harvesting (bath controls 1 and 2), and reverse transcriptase was omitted from one cell (−RT control). cDNA from total organ of Corti was used as a template to control amplification of the individual TaqMan assays (positive control).

Transfection, Patch-clamp, photolysis of caged Ca^{2+} and measurements of $[Ca^{2+}]_i$, total internal reflection microscopy (TIRFM) of chromaffin cells

Bovine and mouse adrenal chromaffin cells were prepared as described (Smith et al., 1998; Sorensen et al., 2003). A semliki forest virus (SFV) was used to transfect chromaffin cells with cDNA encoding for otoferlin with C-terminal fusion to eGFP (Otof-eGFP). The SFV was produced as described (Berglund et al., 1993; Smerdou and Liljestrom, 1999). Cells were transfected 1 day after plating and used for analysis 24 h later. Cells were chosen for physiological analysis by their GFP-fluorescence (preferring intermediate fluorescence). A Nikon TE-2000 microscope equipped with the NIKON TIRF-condensor and a 1.45 NA objective was combined with a Picarro Cyan laser (488 nm, 20 mW) and an Andor iXon 887 BI CCD for “through the lens TIRFM”. The laser beam was focused onto the back focal plane of the objective and moved off-axis to obtain total reflection at the glass-water interface. The resulting evanescent field allowed for a selective excitation of near-plasma-membrane fluorescence. One pixel of the CCD represented 107 nm in the image plane. Images were acquired at 100 Hz without stimulation of the chromaffin cells.

Whole-cell recordings were carried out with 5–6 MΩ pipettes using an EPC-9 patch-clamp amplifier together with “Pulse” software. The pipette solution contained (in mM) 100 Cs-

glutamate, 8 NaCl, 2 Mg-ATP, 0.3 Na2-GTP, 32 Cs-HEPES, 5 nitrophenyl-EGTA (NP-EGTA), 4 CaCl2, 0.3 Furaptra (pH 7.2). The extracellular solution contained (in mM) 145 NaCl, 2.8 KCl, 2 CaCl2, 1 MgCl2, 10 Na-HEPES and 10 glucose (pH 7.4). Capacitance measurements were performed as described above for IHCs. To obtain step-wise increases in $[Ca^{2+}]_i$, short (~1.3 ms) flashes of ultraviolet light from a Xenon arc flash lamp (Rapp OptoElectronics, Hamburg, Germany) were applied to the NP-EGTA-loaded chromaffin cells. $[Ca^{2+}]_i$ was measured by dual-wavelength ratiometric fluorimetry with the indicator dye Furaptra. The dye was excited with light alternating between 350 and 380 nm using a monochromator-illumination based system (TILL photonics, Martinsried, Germany), and the resulting fluorescent signal was measured using a photodiode. $[Ca^{2+}]_i$ was determined from the ratio R of the fluorescent signals at both wavelength as described (Beutner et al., 2001). The isocoefficient, α (Zhou and Neher, 1993), was measured to be 0.1.

Autaptic hippocampal neuron culture, electrophysiology, transduction and morphology

Microisland cultures of hippocampal neurons from $Syt1^{-/-}$ or $Otof^{-/-}$ mice and from wild type controls were prepared as described (Jockusch et al., 2007) and recorded between DIV 10–15. Syt1 deficient neurons were transfected 12 hrs before recordings using an SFV with Otof-eGFP (see chromaffin cells), eGFP or Syt1 with N-terminal fusion to eGFP (eGFP-Syt1). Neurons were whole cell voltage clamped at −70 mV using an axoclamp amplifier under the control of Clampex 10.1 software. All analyses were performed using Axograph 4.1 or Axograph X. EPSCs were evoked by depolarizing the cells to 0 mV. The extracellular saline solution contained (in mM): 140 NaCl, 2.4 KCl, 10 HEPES, 10 glucose, 4 $CaCl_2$ and 4 $MgCl_2$ (320 mOsmol/l, pH 7.3). Pipette solutions contained (in mM): 136 KCl, 17.8 HEPES, 1 EGTA, 4.6 $MgCl_2$, 4 NaATP, 0.3 Na_2GTP, 15 creatine phosphate and 5 U/ml phosphocreatine kinase (315–320 mOsmol/l, pH 7.4). Neurons (cultured until DIV14) were fixed with 4% paraformaldehye in PBS for 20 min and were stained with rabbit anti-Vglut1 (1:1000; SYSY) and mouse anti-otoferlin (1:300; Abcam) and secondary antibodies as described for IHCs.

Data analysis

The data were analyzed using the IgorPro 6 software package (Wavemetrics, Lake Oswego, OR) and Origin 6.0 (Microcal Software, Northampton, MA). Averaged data are expressed as mean ± sem. Significance was tested using the unpaired, two-tailed t-tests, unless stated otherwise. For $Otof^{-/-}$ hippocampal neurons, analysis was performed as described by Jockusch et al. (2007).

Results

Viral transduction of hair cells and targeting of mis-expressed Syt1 to synaptic vesicles

A prerequisite to study a potential functional equivalence of otoferlin and Syt1 in hair cells was to transfect $Otof^{-/-}$ hair cells while maintaining cellular and/or cochlear integrity. Here, we established transduction by adeno-associated virus (AAV) of both postnatal IHCs in cultured organs of Corti (*in vitro* approach) and IHC progenitor cells after microinjection into the embryonic otocyst (*in vivo* approach: Gubbels et al., 2008; Brigande et al., 2009).

Numerous viral vectors (semliki forest virus SF40, lentivirus, combinations of various AAV serotypes and promotors/enhancers) collectively failed to transduce cultured IHCs. Finally, we found a chimeric AAV-1/2 to efficiently transduce IHCs and outer hair cells (OHCs) both *in vitro* and *in vivo* when driving transgene expression by a CMV enhanced human β-actin promoter (Fig. 1A). This virus contains inverted terminal repeats of serotype 2 and capsid proteins of serotypes 1 and 2. To identify Syt1 transfected cells during patch clamp experiments, we co-expressed eGFP via an internal ribosomal entry site within the same

viral construct (Fig. 1A). After *in vitro* application of this AAV-1/2 to cultured organs of Corti (OC) explanted at p8, we found a substantial number of transfected IHCs, though the transduction rate varied significantly between OC cultures. For *in vivo* transduction we microinjected this virus into the otocyst at embryonic days 11.5–12.5. The rate of IHC transduction varied as a function of tonotopy (highest in the low frequency sensing cochlear apex and lowest in the high frequency sensing base) and from experiment to experiment (Table 1), consistent with the findings in a proof of principle study of AAV-mediated gene transfer into the inner ear via injection into the developing otocyst (Bedrosian et al., 2006). In addition, we observed variable expression of the transgene in OHCs and spiral ganglion neurons (data not shown).

The localization of ectopically expressed Syt1 in hair cells after otocyst injection was examined by co-labelling of Syt1 and the vesicular protein Vglut3 and high resolution imaging (confocal and STED microscopy). Confocal images (Fig 1C) and STED images (Fig 1D with lateral and axial resolution of approximately 50 nm and 800 nm for both colors, respectively) showed a similar distribution pattern of Vglut3 and Syt1 in Syt1-transfected IHCs. Deconvolution of STED images revealed a more structured immunolabeling pattern for both Syt1 and Vglut3 (Fig. 1E). Note an efferent nerve ending with endogenous Syt1 immunoreactivity (arrow in Fig 1D) and a part of a non-transfected cell stained for Vglut3 only (arrowhead). Merging of the two color channels revealed a good correlation of the localization of the two antigens within the cytoplasm, whereas Syt1 labels the plasma membrane more intensely than Vglut3 (Fig. 1F). Further, we probed the pixel-wise correlation between the two fluorescence channels in deconvolved STED images of the basolateral end of a hair cell (Fig 1G,H). The correlation coefficient within a region of interest (sketched in Fig. 1F) was 0.686, and it decreased upon lateral shift arguing for a genuine colocalization of the two antigens (Fig 1G). Fluorescence intensity histograms along three lines indicate a similar distribution of Syt1 and Vglut3 within the cell (Fig. 1I).

Functional impact of ectopic expression of Syt1 in IHCs of *Otof*$^{-/-}$ mice

We studied auditory function by recording ABRs in 4–5 week old mice, whose left otocyst had been microinjected with the Syt1-encoding AAV at embryonic day 11.5–12.5 (Bedrosian et al., 2006; Gubbels et al., 2008). Wild-type ears injected with GFP or ears of normal hearing *Otof*$^{+/-}$ animals injected with Syt1 served as controls. Ectopic expression of Syt1 in *Otof*$^{-/-}$ IHCs did not result in any detectable ABR responses as compared to the uninjected contralateral ears (Fig. 2A, right panel), even at 120 dB sound pressure level (SPL), in two independent data sets, which were acquired by different experimenters. As reported previously (Bedrosian et al., 2006), ectopic expression of GFP in hair cells of wild-type mice did not interfere with their hearing (Fig. 2B, left panel). Injection of the Syt1-AAV caused an increase in hearing threshold in one set of experiments (data not shown), the reasons for which are currently unclear. Therefore, and because hearing thresholds in the uninjected wild-type ears were relatively high (Fig. 2B, left panel) we performed the second set of experiments in which we also recorded otoacoustic emissions in order to test for potential changes in OHC-mediated cochlear amplification (Fig. 2A–C). For this, we cross-bred *Otof*$^{-/-}$ with *Otof*$^{+/-}$ mice and injected the same Syt1 encoding AAV into the otocysts of all pups, such that we could test hearing and outer hair cell function in *Otof*$^{-/-}$ and in hearing (*Otof*$^{+/-}$) animals that had been injected within the same experiment. Otoacoustic emissions were detectable in both injected and uninjected ears of both *Otof*$^{+/-}$ and *Otof*$^{-/-}$ mice (Fig. 2C), and hearing thresholds were not significantly different between injected and uninjected ears of *Otof*$^{+/-}$ mice ($p > 0.05$ for all frequencies, Fig. 2B right panel). There was a tendency towards elevated thresholds in the mid-frequency range for which we found low IHC transduction. Low frequency hearing mediated by the cochlear apex was completely unaltered arguing against adverse effects of AAV injection on cochlear function in this

second set of experiments, where we achieved high transduction rates of apical IHCs (~70%). Therefore, despite proper protein targeting, ectopic expression of Syt1 in IHCs does not restore hearing in *Otof*$^{-/-}$ mice, suggesting a continued failure of synaptic transmission in Syt1-expressing *Otof*$^{-/-}$ IHCs.

Differential interference contrast microscopy of IHC and OHC hair bundles and cell bodies further indicated that IHCs were intact in the transfected cochleae (Fig. 3A). Next, we studied the presynaptic function of Syt1-transfected apical IHCs of 4-week-old *Otof*$^{-/-}$ and *Otof*$^{+/+}$ mice by patch-clamp recordings of Ca^{2+} current and membrane capacitance increments (ΔC_m) (Fig. 3B,C). Ectopic expression of Syt1 in *Otof*$^{+/+}$ IHCs did not interfere with Ca^{2+} currents and ΔC_m compared to non-transfected IHCs (Fig. 3C). Still, Syt1-expressing *Otof*$^{-/-}$ IHCs did not show any significant ΔC_m in response to sizeable Ca^{2+} currents (Fig. 3B,C). Thus, exocytosis of mature IHCs in *Otof*$^{-/-}$ mice cannot be restored by ectopic expression of Syt1 in IHCs by *in utero* gene transfer to hair cell progenitors in the embryonic inner ear.

As a complementary approach we transfected p8–9 *Otof*$^{-/-}$ and *Otof*$^{+/+}$ IHCs in organotypic culture using the same virus and patch-clamped them at 6–8 DIV (Fig. 1C, 3D). Just as in non-transfected cultures of *Otof*$^{-/-}$ organs of Corti, exocytosis was nearly abolished in Syt1-overexpressing *Otof*$^{-/-}$ IHCs (Fig. 3D). In summary, neither acute nor chronic ectopic expression of Syt1 restores Ca^{2+}-triggered exocytosis in *Otof*$^{-/-}$ IHCs.

Testing Syt1 function and analyzing Syt isoform expression in IHCs

While the absence of Syt1, 2 and 3 was previously reported for guinea pig IHCs (Safieddine and Wenthold, 1999), a recent study claimed that Syt1 and Syt4 (potentially in combination with Syt2) function as Ca^{2+} sensors for exocytosis in IHCs of immature and mature mice, respectively (Johnson et al., 2010). In another study, a role for Syt1 in immature hair cells was reported, together with the expression of both Syt1 and Syt2 in immature hair cells up to p8 (Beurg et al., 2010). Here, we tested the expression of Syt1 and Syt2 in IHCs by immunolabeling with isoform specific antibodies. We found a very weak staining for Syt1 in the cytosol but not in the basolateral membrane at p3 (Fig. 4A, left). At later developmental stages (p9 or p19) we did not detect Syt1 protein, while Syt1 immunofluorescence was always observed in efferent presynaptic olivocochlear terminals underneath the IHCs serving as an intrinsic positive control of the Syt1 immunolabeling. We detected a weak cytosolic Syt2 immunoreactivity in mouse IHCs at p3 and p9 but not after the onset of hearing (p19; Fig. 4A, right). We then probed the expression of Syt isoforms 1–15 in rat IHCs by single cell real-time-PCR at p12 (Fig. 4E). Consistent with our immunohistochemistry in mice, Syt1 mRNA was absent from rat IHCs. Also, we did not detect Syt4 mRNA in any p12 IHC and in only two out of eighteen IHCs at p14 (data not shown). However, mRNA of some other isoforms were detected, amongst them Syt2, the putative Ca^{2+}-sensor of transmitter release at the calyx of Held synapse (Sun et al., 2007). We found Syt2 mRNA in 80% of the IHCs at p12 (Fig. 4E) but only in 7 of 18 IHCs at p14–16 (data not shown).

Next, we studied exocytosis in IHCs of mice lacking Syt1 using membrane capacitance measurements. As *Syt1*$^{-/-}$ mice die at birth we performed the measurements in cultured organs of Corti of newborn mice after 6 DIV. Depolarization-evoked Ca^{2+} currents and exocytic membrane capacitance (ΔC_m) for up to 200 ms long depolarizations were unaltered in *Syt1*$^{-/-}$ IHCs, indicating that the absence of Syt1 does not impair Ca^{2+}-triggered fusion at the immature IHC synapse (Fig. 4B–D).

Testing targeting and function of otoferlin in adrenal chromaffin cells

Adrenal chromaffin cells represent an established model system of Ca^{2+} regulated exocytosis (Rettig and Neher, 2002). Chromaffin cells release epinephrine from large dense core vesicles (chromaffin granules) upon depolarization or flash photolysis of caged Ca^{2+} and employ a set of synaptic proteins that largely overlaps with the exocytic machinery of neuronal synapses. For example, Syt1 is required for exocytosis of the readily releasable pool (RRP) in chromaffin cells (Voets et al., 2001), which is compatible with a Ca^{2+} sensor function of Syt1 for synchronous exocytosis. Therefore, it seemed sensible to test for potential effects of ectopic otoferlin expression in chromaffin cells. We transfected bovine chromaffin cells with a semliki forest virus encoding otoferlin-eGFP cDNA and analyzed by TIRF microscopy whether otoferlin is targeted to chromaffin granules. The decaying evanescent field spatially restricted excitation of fluorophores to a ~300 nm thin basal layer of the glass-attached chromaffin cell in our set-up. We readily observed diffraction limited fluorescent objects moving in and out the evanescent field in which they stayed for different amounts of time (Fig. 5A) indicating that Otof-eGFP is, indeed, targeted to chromaffin granules (Fig. 5) that visited the near-membrane cytosol. We then carried out whole cell membrane capacitance (C_m) measurements to monitor exocytosis in response to flash photolysis of caged Ca^{2+}. The flash-induced exocytic burst was analyzed using double exponential fitting to the C_m traces over a period of 300 ms. Fast (RRP) and slow (slowly releasable pool) components of the exocytic burst were maintained (Fig. 5B) with comparable kinetics (τ_{fast}(Otof-overexpress.): 11.88 ± 1.37 ms vs. τ_{fast}(control): 13.39 ± 1.23 ms; τ_{slow}(Otof-overexpress.): 242.25 ± 24.16 ms vs. τ_{slow}(control): 235.51 ± 29.55 ms) and amplitudes (A_{fast}(Otof-overexpress.): 173.2 ± 34.69 fF vs. A_{fast} (control): 203.42 ± 29.65; A_{slow}(Otof-overexpress.): 321.02 ± 48.54 fF vs. A_{slow}(control): 270.95 ± 28.03 fF) in transfected cells expressing otoferlin versus in non-transfected cells (same postflash $[Ca^{2+}]_i$: Otof-overexpress. (n=20): 15.67 ± 0.69 vs. control (n=20): 15.64 ± 0.61). Finally, we probed the potential of otoferlin overexpression to restore the synchronous exocytosis in Syt1-deficient mouse chromaffin cells. Syt1-deficiency specifically abolishes the fast component of the exocytic burst (Voets et al., 2001), which remained absent despite overexpression of otoferlin (Fig. 5C). Therefore, otoferlin seems incapable of functionally replacing Syt1 in chromaffin cell exocytosis.

Testing the function of over-expressed otoferlin in Syt1-deficient hippocampal neurons

Next, we expressed Otof-eGFP in hippocampal neurons of *Syt1*$^{-/-}$ mice using the same semliki forest virus as used for chromaffin cells. Expression was confirmed by eGFP fluorescence during the recordings, and on fixed cells by immunofluorescence using an anti-otoferlin antibody (Fig. 6A). Using otoferlin immunolabelling in cultured non-transfected hippocampal neurons, we did not detect immunofluorescence above that found in *Otof*$^{-/-}$ neurons (data not shown). Upon virus transduction to induce overexpression of otoferlin, co-staining with the presynaptic protein Vglut1 showed a spot-like distribution for both antigens, however otoferlin immunolabeling appeared juxtaposed to the presynaptic boutons. We did not observe rescue of synchronous synaptic transmission in *Syt1*$^{-/-}$ neurons overexpressing Otof-eGFP, while it was restored by semliki forest virus-mediated expression of eGFP-Syt1 (Fig. 6B–D). However, there was an increase in asynchronous release in otoferlin-overexpressing *Syt1*$^{-/-}$ neurons (Fig. 6B), leading to a larger total excitatory postsynaptic current (EPSC) charge in otoferlin-overexpressing *Syt1*$^{-/-}$ neurons compared to GFP-transfected neurons (Fig. 6E). Further, we found the amplitude of mEPSCs to be slightly higher in otoferlin-overexpressing *Syt1*$^{-/-}$ neurons [25.93 ± 2.24 pA (n = 25) compared to 18.87 ± 1.06 pA (n = 17) in Syt1-transduced neurons), such that an increase in the number of postsynaptic AMPA receptors might have contributed to the larger EPSC charge.

Functional analysis of otoferlin-deficient hippocampal neurons

We next studied spontaneous and evoked exocytosis in *Otof*$^{-/-}$ autaptic hippocampal neurons to test for a potential role of endogenous otoferlin that might have escaped detection in our immunhistochemistry (Fig 7). No difference was detected in EPSC amplitude, EPSC charge (Fig. 7A), readily realeasable pool (RRP) charge (measured during application of 0.5 M sucrose, Fig. 7C) or vesicular release probability P_{vr} (calculated as EPSC charge divided by RRP charge) between *Otof*$^{+/+}$ and *Otof*$^{-/-}$ hippocampal neurons. Further, mEPSC amplitude or mEPSC frequency were unchanged between hippocampal neurons of the two genotypes (Fig. 7D). Thus, at least under these *in vitro* conditions, lack of otoferlin does not affect presynaptic function in hippocampal neurons.

Discussion

In this study we tested for functional equivalence of Syt1 and the hair cell C_2-domain protein otoferlin. Despite a similar behaviour of both proteins in biochemical experiments (Johnson and Chapman, 2010), we found that expression of Syt1 in IHCs cannot restore hair cell exocytosis in mice lacking otoferlin. Likewise, overexpression of otoferlin in chromaffin cells or hippocampal neurons did not rescue synchronous synaptic transmission in mice lacking Syt1. While future site-directed mutagenesis studies need to scrutinize the putative Ca^{2+} sensor function of otoferlin in synaptic vesicle fusion in IHCs, our study demonstrates that it cannot simply be replaced by Syt1. Different from many other systems, cochlear hair cells have rarely if ever been used for exploring molecular structure-function relationships by viral gene transfer. This study demonstrated efficient *in vitro* and *in vivo* transduction procedures and revealed normal presynaptic properties of wild-type hair cells expressing the transgenes five weeks after transduction, paving the way for future site-directed mutagenesis studies of synaptic proteins in hair cells.

Block of exocytosis in *Otof*$^{-/-}$ IHCs despite expression of Syt2 and Syt1

The identity of the Ca^{2+} sensor(s) of hair cell exocytosis is the subject of current controversy. Our analysis of synaptotagmin expression in IHCs supports the conclusion of Safieddine and Wenthold (1999) and Beurg et al. (2010) that Syt1, 2 and 3 are absent in mature IHCs. The transient expression of Syt2 seems not to be critical for exocytosis in immature IHCs (Beurg et al., 2010), and does not enable exocytosis in *Otof*$^{-/-}$ IHCs, which is nearly abolished from p4 onward (Roux et al., 2006; Beurg et al., 2010; this study). The lack of Syt4 mRNA from p12 rat IHCs contrasts with a recent study on the role of Syt4 in mouse IHCs (Johnson et al., 2010). suggested that Syt4 serves as the Ca^{2+} sensor of exocytosis in mature mouse IHCs, potentially together with Syt2, questioning the hypothesis that otoferlin acts as the specialized Ca^{2+} sensor of exocytosis in IHCs. While we could hardly detect Syt4 mRNA in single hair cells, accumulating biochemical evidence points towards a Syt1-like function of otoferlin (Johnson and Chapman, 2010). Our demonstration that the canonical Ca^{2+} sensor Syt1 cannot rescue exocytosis in otoferlin-deficient IHCs seemingly argues against a Ca^{2+} sensing function of otoferlin in IHC transmitter release. However, the rescue approach may have failed in spite of a role of otoferlin as Ca^{2+} sensor of vesicle fusion in IHCs: Firstly, upstream functions of otoferlin in IHCs such as vesicle supply (Pangrsic et al., 2010) may not have been supported by Syt1, and secondly, absence of facilitating proteins like complexins (Strenzke et al., 2009) or of Syt1 interaction partners could have precluded Syt1 functionality. The finding that ABRs could not be elicited in the Syt1-AAV-1/2 injected *Otof*$^{-/-}$ ears was most likely related to the remaining block of IHC exocytosis and not caused by too few transduced IHCs. If the 70% of the apical IHCs that expressed Syt1 were releasing transmitter in response, we would expect some ABR at least for low sound frequency stimulation as the ABR amplitude declines nearly linearly when the

numbers of IHCs and spiral ganglion neurons are reduced by carboplatin application to the cochlea of chincillas (Ding et al., 1999).

In case of the mirror experiment, the overexpression of otoferlin in *Syt1*$^{-/-}$ hippocampal neurons, we cannot exclude that failure to rescue synchronous vesicle release in hippocampal neurons might be due to mistargeting of over-expressed otoferlin, as it seems not to be primarily targeted to Vglut1 immunolabeled presynapses. By contrast, in chromaffin cells proper targeting of otoferlin was indicated by labeling of the granules and still we observed a failure to rescue fast exocytosis. However, the C-terminal fusion to eGFP might have impaired otoferlin's function, although the fluorophore is tagged to the intravesicular site of the protein which did not interfere with function in the case of Syt1 (Han et al., 2005). For both *Syt1*$^{-/-}$ chromaffin cells and hippocampal neurons, failure of rescue by otoferlin may have resulted from lack of otoferlininteracting proteins required for exocytosis in both cell types or for presynaptic targeting in case of hippocampal neurons.

Auditory function following AAV-mediated gene transfer to the embryonic ear

Gene transfer into mature cochlear hair cells has remained challenging (for reviews see Brigande and Heller, 2009; Luebke et al., 2009; Wei and Yamoah, 2009). Here we demonstrate efficient viral transgene expression in IHCs and OHCs *in vitro* and *in vivo* using an AAV-1/2 vector carrying our gene of interest under the control of a CMV enhanced β-actin promotor. Wild-type IHCs transfected by transuterine injection of AAV-1/2 presented mature stereocilliar bundle and cell body morphologies, and intact Ca^{2+} currents and exocytosis in the 4th postnatal week. Together with the normal ABR recordings in mice up to 5 weeks of age misexpressing eGFP in IHCs, OHCs and spiral ganglion neurons, these data suggest that the AAV-1/2 vector may be a suitable tool for therapeutic gene delivery to IHCs. We found increased ABR thresholds in the first set of Syt1-AAV-1/2 injected ears, which showed higher transfection rates in the middle and the basal parts of the cochlea than seen in the second set. We cannot exclude the possibility that ectopic Syt1-expression in hair cells causes auditory dysfunction but think that our patch-clamp data from the first set of injected ears and the near-normal auditory systems physiology in the second set of Syt1-AAV-1/2 injected ears argue against it. Clearly, rescue experiments will be most conclusive at the level of auditory population responses such as ABRs, if (1) little degeneration has occurred, (2) transduction is efficient, (3) the hearing loss of the non-rescued mutant is severe and the background strain shows good hearing. Unfortunately, the coding sequences of several deafness genes, including *Otof*, exceed the packaging capacity of AAV vectors, underlining the need to identify viral vectors with significantly larger capacities.

Acknowledgments

This study was designed by T.M., E.R., J. Brigande and J.S.R. The experimental work was performed by E.R. (*Otof*$^{-/-}$ mice, immuno, single cell PCR, *in vitro* transduction and patch-clamp), C.B., K.R. (*in utero* gene transfer, quantification of transfected hair cells, auditory brainstem responses), J.N. (patch-clamp, immuno of hair cells), R. Nair (patch-clamp, immuno of neurons), M.K., R. Nouvian (patch-clamp of chromaffin cells), A.B. (establishing in vitro transduction and immuno, generation of virus together with S.K.), S.K. (generation of virus), J. Brigande (*in utero* gene transfer) and J. Bückers, L.K. and S.W.H. (high resolution STED imaging). I.R. and C.P. subcloned full length otoferlin cDNA for viral transduction. The manuscript was prepared by T.M, E.R., J. Brigande. and J.N.. We would like to thank R. Nehring and D. Reuter for production of the SLV and transduction of chromaffin cells and S. Anderson for help with the TIRFM. We thank Rebecca Medda and Mark Rutherford for advice regarding immunostaining for STED microscopy, and Aaron B. Wong for help with image analysis. We thank Thomas C. Südhof for providing the *Syt1*$^{-/-}$ mice and Peter Jonas for synaptotagmin primers and taqman probes. We thank Nadine Herrmann, Anja Galinski and Nina Dankenbrink-Werder for expert technical assistance. This work was supported by grants of the Max Planck Society (Tandem-Project grant to N.B. and T.M.), the German Federal Ministry of Education and Research (Bernstein Center grant 01GQ0433 to T.M.), the Center for Molecular Physiology of the Brain (FZT-103 to S.K., N.B. and T.M.) and the National Institute on Deafness and Other Communication Disorders (NIH R01DC8595 to J.B. and P30 DC005983).

References

Bedrosian JC, Gratton MA, Brigande JV, Tang W, Landau J, Bennett J. In vivo delivery of recombinant viruses to the fetal murine cochlea: transduction characteristics and long-term effects on auditory function. Mol Ther. 2006; 14:328–335. [PubMed: 16765094]

Berglund P, Sjoberg M, Garoff H, Atkins GJ, Sheahan BJ, Liljestrom P. Semliki Forest virus expression system: production of conditionally infectious recombinant particles. Biotechnology (N Y). 1993; 11:916–920. [PubMed: 7688971]

Beurg M, Michalski N, Safieddine S, Bouleau Y, Schneggenburger R, Chapman ER, Petit C, Dulon D. Control of exocytosis by synaptotagmins and otoferlin in auditory hair cells. J Neurosci. 2010; 30:13281–13290. [PubMed: 20926654]

Beutner D, Voets T, Neher E, Moser T. Calcium dependence of exocytosis and endocytosis at the cochlear inner hair cell afferent synapse. Neuron. 2001; 29:681–690. [PubMed: 11301027]

Brigande JV, Heller S. Quo vadis, hair cell regeneration? Nat Neurosci. 2009; 12:679–685. [PubMed: 19471265]

Brigande JV, Gubbels SP, Woessner DW, Jungwirth JJ, Bresee CS. Electroporation-mediated gene transfer to the developing mouse inner ear. Methods Mol Biol. 2009; 493:125–139. [PubMed: 18839345]

Chieregatti E, Witkin JW, Baldini G. SNAP-25 and synaptotagmin 1 function in Ca2+-dependent reversible docking of granules to the plasma membrane. Traffic. 2002; 3:496–511. [PubMed: 12047557]

Cho W, Stahelin RV. Membrane-protein interactions in cell signaling and membrane trafficking. Annu Rev Biophys Biomol Struct. 2005; 34:119–151. [PubMed: 15869386]

de Wit H, Walter AM, Milosevic I, Gulyas-Kovacs A, Riedel D, Sorensen JB, Verhage M. Synaptotagmin-1 docks secretory vesicles to syntaxin-1/SNAP-25 acceptor complexes. Cell. 2009; 138:935–946. [PubMed: 19716167]

Ding DL, Wang J, Salvi R, Henderson D, Hu BH, McFadden SL, Mueller M. Selective loss of inner hair cells and type-I ganglion neurons in carboplatin-treated chinchillas. Mechanisms of damage and protection. Ann N Y Acad Sci. 1999; 884:152–170. [PubMed: 10842592]

Gubbels SP, Woessner DW, Mitchell JC, Ricci AJ, Brigande JV. Functional auditory hair cells produced in the mammalian cochlea by in utero gene transfer. Nature. 2008

Han W, Rhee JS, Maximov A, Lin W, Hammer RE, Rosenmund C, Sudhof TC. C-terminal ECFP fusion impairs synaptotagmin 1 function: crowding out synaptotagmin 1. J Biol Chem. 2005; 280:5089–5100. [PubMed: 15561725]

Heidrych P, Zimmermann U, Kuhn S, Franz C, Engel J, Duncker SV, Hirt B, Pusch CM, Ruth P, Pfister M, Marcotti W, Blin N, Knipper M. Otoferlin interacts with myosin VI: implications for maintenance of the basolateral synaptic structure of the inner hair cell. Hum Mol Genet. 2009; 18:2779–2790. [PubMed: 19417007]

Holmes TJ, Liu Y-H. Richardson-Lucy/maximum likelihood image restoration algorithm for fluorescence microscopy: further testing. Appl Opt. 1989; 28:4930–4938. [PubMed: 20555971]

Jockusch WJ, Speidel D, Sigler A, Sorensen JB, Varoqueaux F, Rhee JS, Brose N. CAPS-1 and CAPS-2 are essential synaptic vesicle priming proteins. Cell. 2007; 131:796–808. [PubMed: 18022372]

Johnson CP, Chapman ER. Otoferlin is a calcium sensor that directly regulates SNARE-mediated membrane fusion. J Cell Biol. 2010; 191:187–197. [PubMed: 20921140]

Johnson SL, Franz C, Kuhn S, Furness DN, Ruttiger L, Munkner S, Rivolta MN, Seward EP, Herschman HR, Engel J, Knipper M, Marcotti W. Synaptotagmin IV determines the linear Ca2+ dependence of vesicle fusion at auditory ribbon synapses. Nat Neurosci. 2010; 13:45–52. [PubMed: 20010821]

Kerr AM, Reisinger E, Jonas P. Differential dependence of phasic transmitter release on synaptotagmin 1 at GABAergic and glutamatergic hippocampal synapses. Proc Natl Acad Sci U S A. 2008; 105:15581–15586. [PubMed: 18832148]

Khimich D, Nouvian R, Pujol R, Tom Dieck S, Egner A, Gundelfinger ED, Moser T. Hair cell synaptic ribbons are essential for synchronous auditory signalling. Nature. 2005; 434:889–894. [PubMed: 15829963]

Kugler S, Hahnewald R, Garrido M, Reiss J. Long-term rescue of a lethal inherited disease by adeno-associated virus-mediated gene transfer in a mouse model of molybdenum-cofactor deficiency. Am J Hum Genet. 2007; 80:291–297. [PubMed: 17236133]

Luebke AE, Rova C, Von Doersten PG, Poulsen DJ. Adenoviral and AAV-mediated gene transfer to the inner ear: role of serotype, promoter, and viral load on in vivo and in vitro infection efficiencies. Adv Otorhinolaryngol. 2009; 66:87–98. [PubMed: 19494574]

Martens S, McMahon HT. Mechanisms of membrane fusion: disparate players and common principles. Nat Rev Mol Cell Biol. 2008; 9:543–556. [PubMed: 18496517]

McNeil PL, Kirchhausen T. An emergency response team for membrane repair. Nat Rev Mol Cell Biol. 2005; 6:499–505. [PubMed: 15928713]

Moser T, Beutner D. Kinetics of exocytosis and endocytosis at the cochlear inner hair cell afferent synapse of the mouse. Proc Natl Acad Sci U S A. 2000; 97:883–888. [PubMed: 10639174]

Neef J, Gehrt A, Bulankina AV, Meyer AC, Riedel D, Gregg RG, Strenzke N, Moser T. The Ca2+ channel subunit beta2 regulates Ca2+ channel abundance and function in inner hair cells and is required for hearing. J Neurosci. 2009; 29:10730–10740. [PubMed: 19710324]

Nicholson-Tomishima K, Ryan TA. Kinetic efficiency of endocytosis at mammalian CNS synapses requires synaptotagmin I. Proc Natl Acad Sci U S A. 2004; 101:16648–16652. [PubMed: 15492212]

Pangrsic T, Lasarow L, Reuter K, Takago H, Schwander M, Riedel D, Frank T, Tarantino LM, Bailey JS, Strenzke N, Brose N, Muller U, Reisinger E, Moser T. Hearing requires otoferlin-dependent efficient replenishment of synaptic vesicles in hair cells. Nat Neurosci. 2010; 13:869–876. [PubMed: 20562868]

Ramakrishnan NA, Drescher MJ, Drescher DG. Direct interaction of otoferlin with syntaxin 1A, SNAP-25, and the L-type voltage-gated calcium channel Cav1.3. J Biol Chem. 2009; 284:1364–1372. [PubMed: 19004828]

Rettig J, Neher E. Emerging roles of presynaptic proteins in Ca++-triggered exocytosis. Science. 2002; 298:781–785. [PubMed: 12399579]

Rizo J, Sudhof TC. C2-domains, structure and function of a universal Ca2+-binding domain. J Biol Chem. 1998; 273:15879–15882. [PubMed: 9632630]

Roux I, Hosie S, Johnson SL, Bahloul A, Cayet N, Nouaille S, Kros CJ, Petit C, Safieddine S. Myosin VI is required for the proper maturation and function of inner hair cell ribbon synapses. Hum Mol Genet. 2009; 18:4615–4628. [PubMed: 19744958]

Roux I, Safieddine S, Nouvian R, Grati M, Simmler MC, Bahloul A, Perfettini I, Le Gall M, Rostaing P, Hamard G, Triller A, Avan P, Moser T, Petit C. Otoferlin, defective in a human deafness form, is essential for exocytosis at the auditory ribbon synapse. Cell. 2006; 127:277–289. [PubMed: 17055430]

Safieddine S, Wenthold RJ. SNARE complex at the ribbon synapses of cochlear hair cells: analysis of synaptic vesicle- and synaptic membrane-associated proteins. Eur J Neurosci. 1999; 11:803–812. [PubMed: 10103074]

Schwander M, Sczaniecka A, Grillet N, Bailey JS, Avenarius M, Najmabadi H, Steffy BM, Federe GC, Lagler EA, Banan R, Hice R, Grabowski-Boase L, Keithley EM, Ryan AF, Housley GD, Wiltshire T, Smith RJ, Tarantino LM, Muller U. A forward genetics screen in mice identifies recessive deafness traits and reveals that pejvakin is essential for outer hair cell function. J Neurosci. 2007; 27:2163–2175. [PubMed: 17329413]

Smerdou C, Liljestrom P. Two-helper RNA system for production of recombinant Semliki forest virus particles. J Virol. 1999; 73:1092–1098. [PubMed: 9882310]

Smith C, Moser T, Xu T, Neher E. Cytosolic Ca2+ acts by two separate pathways to modulate the supply of release-competent vesicles in chromaffin cells. Neuron. 1998; 20:1243–1253. [PubMed: 9655511]

Sorensen JB, Nagy G, Varoqueaux F, Nehring RB, Brose N, Wilson MC, Neher E. Differential control of the releasable vesicle pools by SNAP-25 splice variants and SNAP-23. Cell. 2003; 114:75–86. [PubMed: 12859899]

Staudt T, Lang MC, Medda R, Engelhardt J, Hell SW. 2,2'-thiodiethanol: a new water soluble mounting medium for high resolution optical microscopy. Microsc Res Tech. 2007; 70:1–9. [PubMed: 17131355]

Strenzke N, Chanda S, Kopp-Scheinpflug C, Khimich D, Reim K, Bulankina AV, Neef A, Wolf F, Brose N, Xu-Friedman MA, Moser T. Complexin-I is required for high-fidelity transmission at the endbulb of held auditory synapse. J Neurosci. 2009; 29:7991–8004. [PubMed: 19553439]

Sun J, Pang ZP, Qin D, Fahim AT, Adachi R, Sudhof TC. A dual-Ca2+-sensor model for neurotransmitter release in a central synapse. Nature. 2007; 450:676–682. [PubMed: 18046404]

Voets T, Moser T, Lund PE, Chow RH, Geppert M, Sudhof TC, Neher E. Intracellular calcium dependence of large dense-core vesicle exocytosis in the absence of synaptotagmin I. Proc Natl Acad Sci U S A. 2001; 98:11680–11685. [PubMed: 11562488]

Wei D, Yamoah EN. Regeneration of the mammalian inner ear sensory epithelium. Curr Opin Otolaryngol Head Neck Surg. 2009; 17:373–380. [PubMed: 19617827]

Young SM Jr, Neher E. Synaptotagmin has an essential function in synaptic vesicle positioning for synchronous release in addition to its role as a calcium sensor. Neuron. 2009; 63:482–496. [PubMed: 19709630]

Zhou Z, Neher E. Mobile and immobile calcium buffers in bovine adrenal chromaffin cells. J Physiol. 1993; 469:245–273. [PubMed: 8271200]

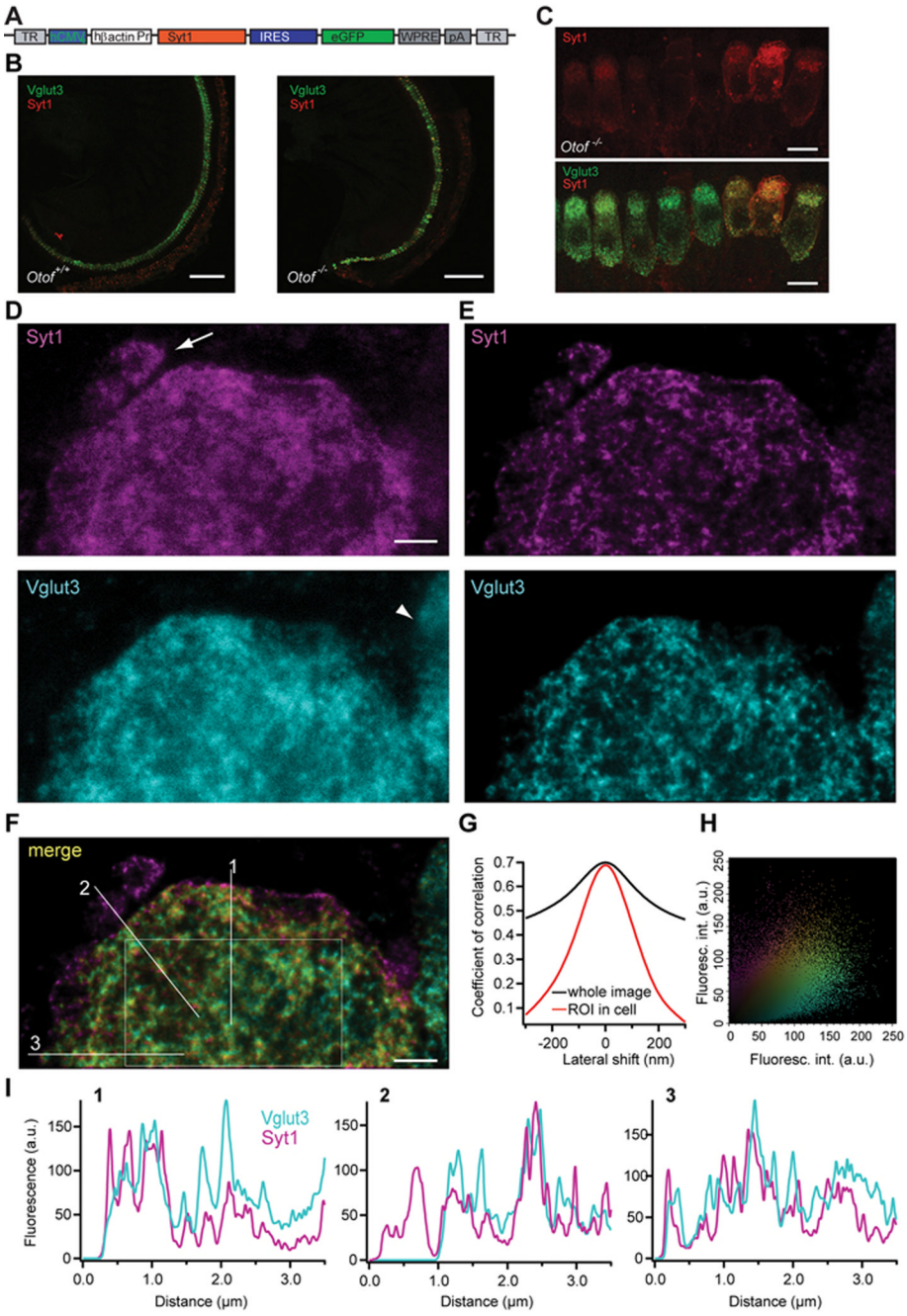

Figure 1. Syt1 is properly targeted in IHCs after AAV-mediated gene transfer

A, layout of the AAV-1/2 Syt1-IRES-eGFP construct.

B, projections of low-resolution confocal sections of wild-type and *Otof*$^{-/-}$ organs of Corti following transuterine injection of the embryonic otocyst using AAV-1/2 Syt1-IRES-eGFP, immunolabeled for Syt1 (red) and Vglut3 (green). Scale bar 100 µm.

C, projections of confocal sections of immunolabeled organs of Corti of *Otof*$^{-/-}$ 7 days after viral Syt1 transduction. Scale bar 10 µm.

D, high resolution two-colour STED imaging of the basal pole of one virus-transfected IHC immunolabeled for Syt1 and Vglut3; Scale bar 1 µm. Image resolution is 50 nm in lateral and 800 nm in axial direction, pictures are background subtracted.. Note the afferent bouton

stained for endogenous Syt1 only (arrow) and the adjacent non-transfected IHC with only Vglut3 labeling (arrowhead).

E, the pictures in ***D*** were deconvoluted using the Richardson-Lucy algorithm (Holmes and Liu, 1989) with 25 iterations and a regularization parameter of 10^{-10}.

F, merge of the pictures from ***E***. Sole Syt1 staining is indicated in magenta, Vglut3 staining in cyan. The colour spectrum indicates the weighted contribution of both channels, with yellow indicating equal fluorescence intensity in both channels.

G, the Pearson correlation coefficient is reduced by a lateral shift of the images from both channels, less severely for the whole image (black line) and more obviously for the region of interest as indicated in ***F*** (red line).

H, fluorescence intensity for Syt1 in one pixel of ***F*** is plotted against the fluorescence intensity derived from Vglut3 immunofluorescence in the same pixel. Colour coding as in ***F***.

I, Fluorescence intensity histogram in both colour channels along the three lines sketched in ***F***.

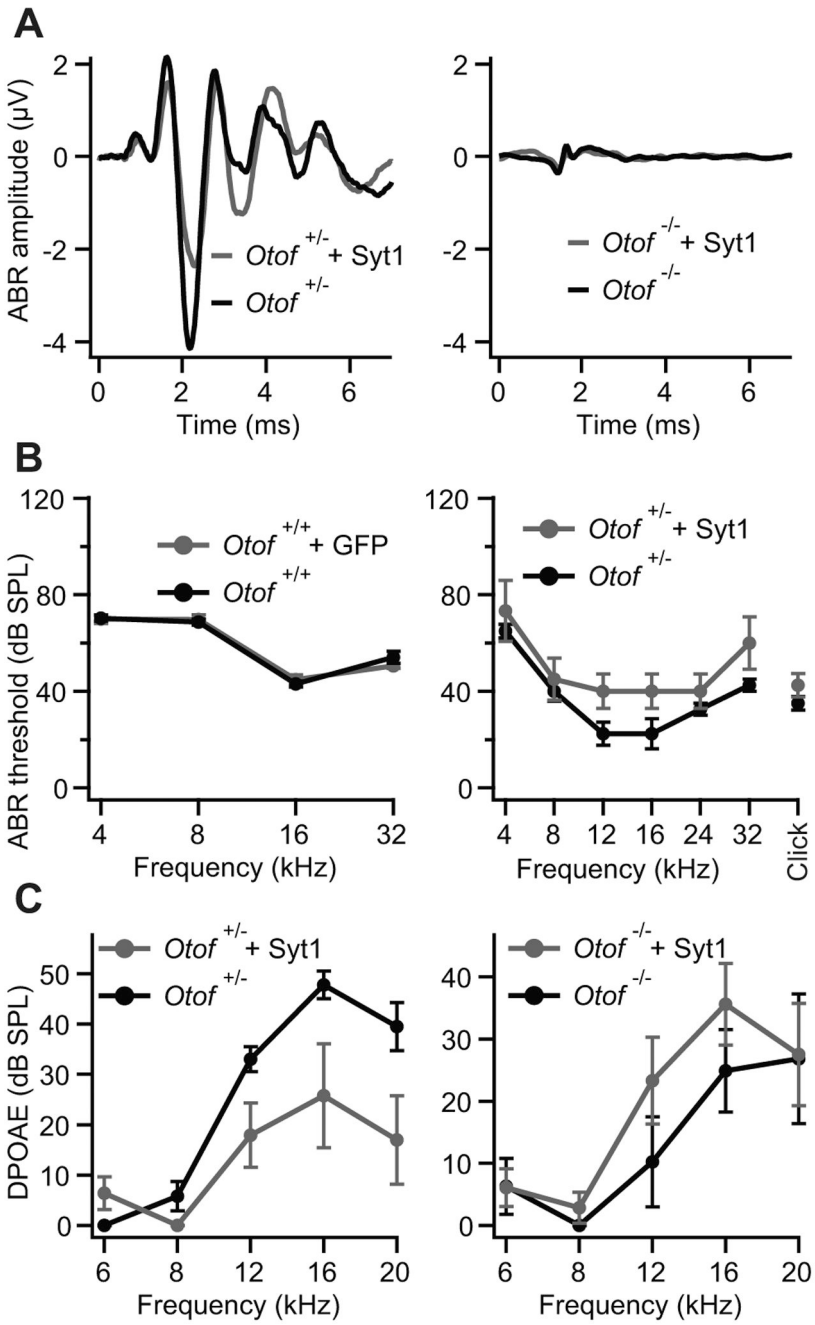

Figure 2. Syt1 does not restore hearing of *Otof*$^{-/-}$ mice

A, auditory brainstem responses. Left panel: mean ABR traces of non-injected (black) and Syt1-AAV injected (grey) ears of *Otof*$^{+/-}$ animals (n = 4) in response to 80 dB SPL; right panel, mean ABR traces of *Otof*$^{-/-}$ animals of which one ear was transfected with Syt1 (grey) and the non-injected contralateral ear served as control (black, n = 4) in response to 100 dB SPL.

B, left panel: mean ABR thresholds and standard errors (sem, n = 25) of non-injected and eGFP-transfected wild type animals (C57B6J). Right panel: mean ABR thresholds and sem (n = 4) of non-injected and Syt1-transfected *Otof*$^{+/-}$ mice. In both independent sets of virus

transduction, no ABR response could be detected in non-injected and in Syt1-transfected *Otof*$^{-/-}$ mice for sound pressure levels (SPL) up to 120 dB (n = 29).
C, outer hair cell function was confirmed by DPOAEs for *Otof*$^{+/-}$ and *Otof*$^{-/-}$ mice (same animals as in right panel of ***B***). While in *Otof*$^{+/-}$ mice the DPOAEs were slightly worse after virus injection (left panel) and might be a reason for the slightly elevated ABR thresholds in ***B***, DPOAEs in *Otof*$^{-/-}$ seem not to be affected by virus transduction (right panel).

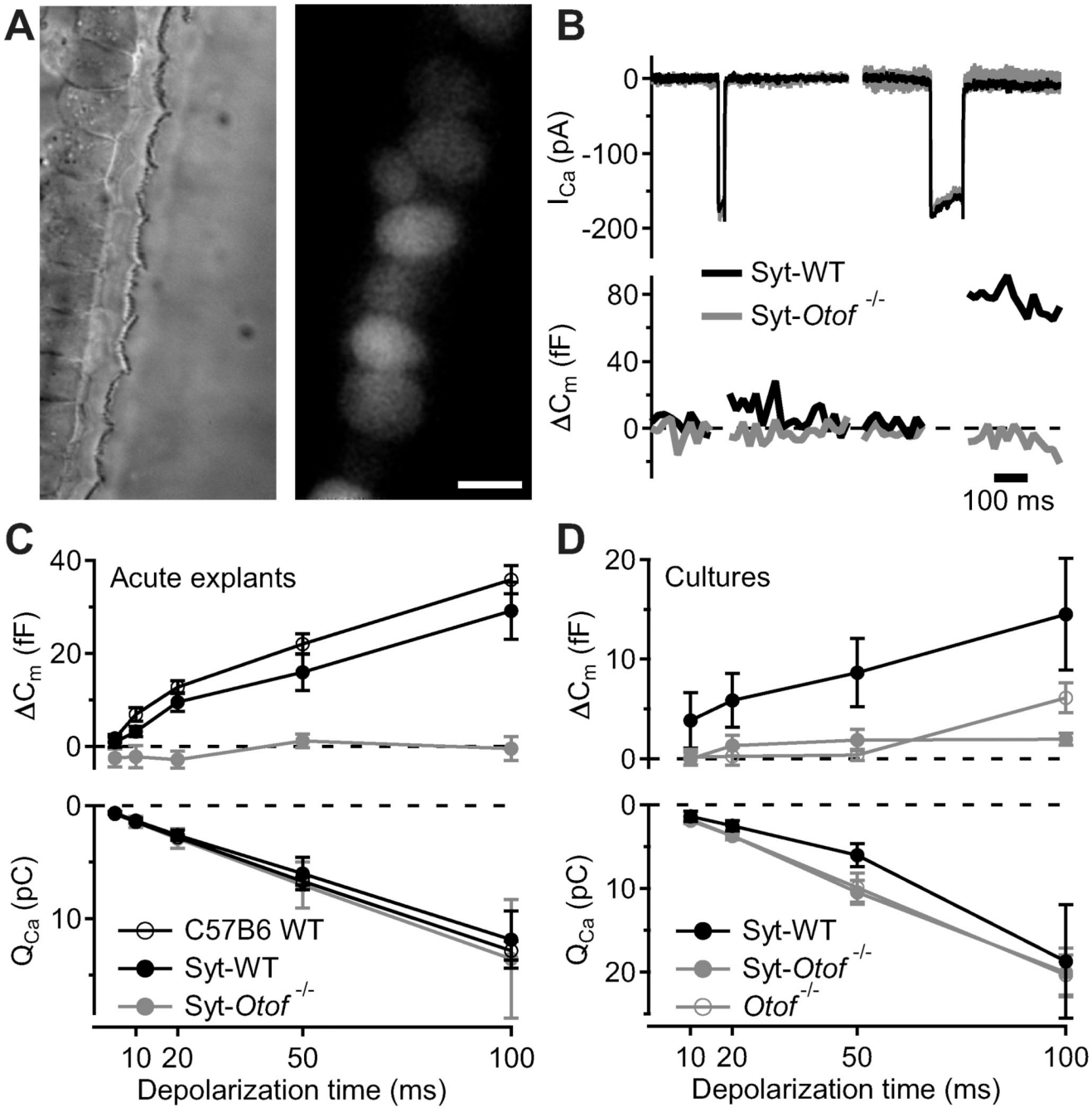

Figure 3. Syt1 overexpression by *in vivo* and *in vitro* AAV transduction do not restore exocytosis in IHCs of *Otof*$^{-/-}$ mice

A, representative differential interference contrast (left) and fluorescence (right) images of p35 IHCs following transuterine transduction of the embryonic otocyst using AAV-1/2 Syt1-IRES-eGFP: preserved stereocilia and high transduction rate (chain of eGFP-positive IHC somata). Scale bar 5 μm.

B, synaptic function in Syt1 misexpressing IHCs in acutely isolated p35 organs of Corti. Representative I_{Ca} currents (top) and ΔC_m in response to a 20 ms (left) and 100 ms (right) depolarization to −14 mV, recorded in perforated-patch configuration from IHCs of wild-

type (black, CD1) and *Otof*$^{-/-}$ mice (grey, mixed background) that had been transfected *in utero*.

C, mean ΔC_m (top) and Q_{Ca} (bottom) responses of untransfected 4–week-old C57B6J IHCs (open circles, n = 12), AAV-1/2 Syt1-IRES-eGFP-transfected CD1 IHCs (filled black circles, n = 9) and AAV-1/2 Syt1-IRES-eGFP-transfected *Otof*$^{-/-}$ IHCs (filled grey circles, n = 6), experiments as in ***B***.

D, mean ΔC_m (top) and Q_{Ca} (bottom) responses of IHCs from *in vitro* AAV-1/2 Syt1-IRES-eGFP transfected cultures of C57B6J and *Otof*$^{-/-}$ organs of Corti, experiments as in ***B*** but ruptured patch in the presence of 10 mM $[Ca^{2+}]_e$.

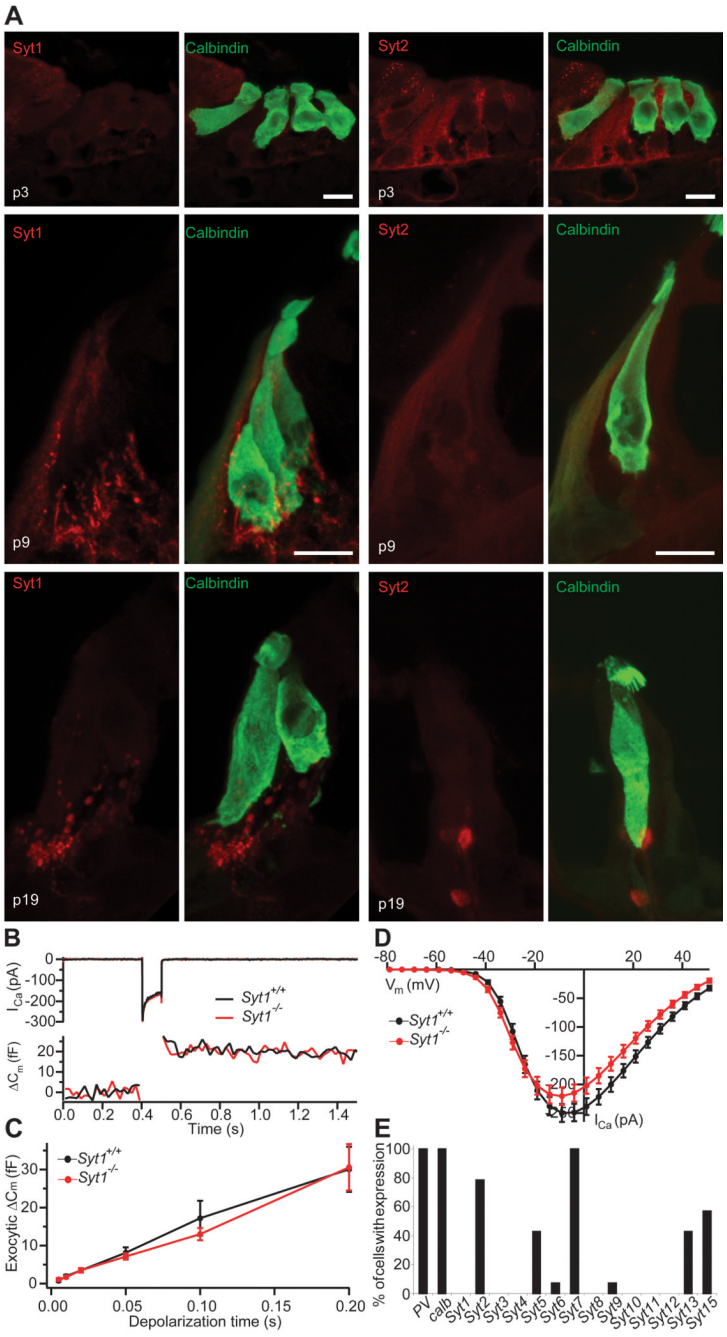

Figure 4. Syt expression analysis and presynaptic hair cell function in *Syt1*$^{-/-}$ mice

A, projection of confocal sections of cryosectioned wild-type organs of Corti from p3 (top), p9 (middle) and p19 (bottom) immunolabeled for calbindin (hair cell marker) and Syt1 (left panels) or Syt2 (right panels). Scale bar: 10 μm.

B, representative I_{Ca} currents (top) and ΔC_m (bottom) in response to 100 ms depolarization to −10 mV recorded in perforated-patch configuration from IHCs in cultures of neonatal organs of Corti from a *Syt1*$^{-/-}$ mouse and a *Syt1*$^{+/+}$ littermate (cultured at p0, DIV 6).

C, mean ΔC_m as a function of stimulus duration for *Syt1*$^{+/+}$ (n = 22) and *Syt1*$^{-/-}$ (n = 16) IHCs recorded as in ***B***.

D, Ca^{2+} current-voltage relationship of *Syt1*$^{+/+}$ (n = 23) and *Syt1*$^{-/-}$ (n = 16) IHCs

E, Expression of 14 Syt isoforms was tested by single cell PCR in 14 IHCs from p12 rats.

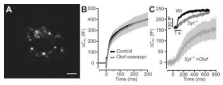

Figure 5. Overexpression of otoferlin in chromaffin cells does not change kinetics or amount of exocytosis and does not restore synchronous exocytosis in Syt1 deficient cells

A, TIRF image of the footprint of a chromaffin cell, which had been transfected with a otoferlin-eGFP fusion construct. Individual fluorescent spots most probably represent otoferlin-eGFP-tagged chromaffin granules, scale bar: 1 μm.

B, average ΔC_m in response to the first flash in control (n = 20; black) and otoferlin-expressing (n = 20; red) bovine chromaffin cells. The first flash was delivered 120–180 s after establishment of the whole-cell configuration.

C, exocytic responses of a wild-type non-transfected mouse chromaffin cell (black) and mean response of 5 Syt1 deficient chromaffin cells that had been transfected to express the otoferline-GFP fusion construct: lack of the fast component of the exocytic burst. Insert: representative exocytotic response from wild-type (black, postflash $[Ca^{2+}]_i$: 16.31 μM) and Syt1 knock-out (red, postflash $[Ca^{2+}]_i$: 15.5 μM).

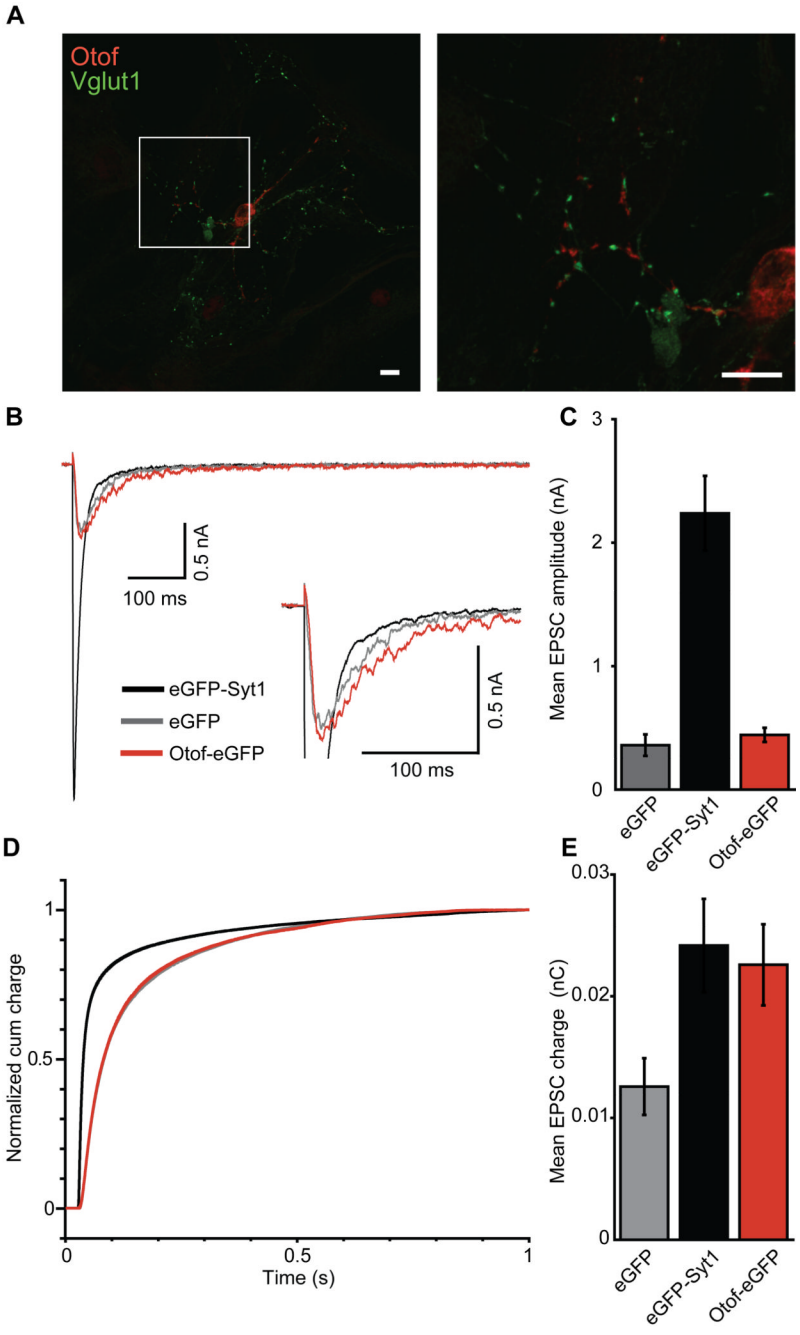

Figure 6. Otoferlin overexpression does not rescue synchronous transmitter release in *Syt1*$^{-/-}$ neurons

A, immunostaining of wild-type autaptic hippocampal neurons transfected with semliki forest virus carrying cDNA for Otof-eGFP. Scale bar 10 µm. Otoferlin immunolabeling appears juxtaposed to Vglut1-immunolabeled presynaptic terminals.

B, average EPSCs of *Syt1*$^{-/-}$ neurons (10–15 DIV, n = 25 each) that were kept as autaptic neuronal cultures for 10 to 15 days and transfected 12 h before recordings with a semliki forest virus encoding for eGFP-Syt1 (black), eGFP (grey) or Otof-eGFP (red).

C, quantification of mean EPSC amplitudes from ***B***.

D, normalized EPSC integrals over time reveal a fast postsynaptic current for Syt1$^{-/-}$ neurons that had been transfected with eGFP-Syt1 (black), but not for Syt1$^{-/-}$ neurons expressing Otof-eGFP (red) or eGFP alone (grey).
E, mean EPSC integral: the evoked postsynaptic charge was increased by overexpression of Otof-eGFP or eGFP-Syt1, but not eGFP alone, in Syt1-deficient autaptic hippocampal neurons. Note that otoferlin-overexpression increased the charge of the asynchronous component only.

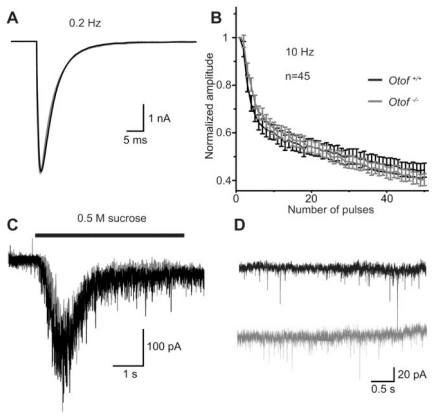

Figure 7. Exocytosis in *Otof*$^{-/-}$ hippocampal neurons

A, representative EPSC traces from *Otof*$^{+/+}$ (black) and *Otof*$^{-/-}$ (grey) autaptic hippocampal neurons at 10 to 15 DIV, elicited by depolarizations to 0 mV for 2 ms at 0.2 Hz.

B, mean normalized amplitudes of EPSCs during a train of action potentials at 10 Hz from *Otof*$^{+/+}$ and *Otof*$^{-/-}$ hippocampal neurons.

C, representative traces showing the release of the readily releasable pool (RRP) induced by application of 0.5 M sucrose.

D, representative traces of miniature EPSC (mEPSCs) in the presence of 300 nM TTX at −70 mV. The frequency and the amplitude of mEPSCs was unchanged in Otof$^{-/-}$ neurons.

Table 1

Percentage of inner and outer hair cells in the Otof$^{-/-}$ and wt cochlea transfected with AAV2/1–2 vector (means ± standard deviation)

	n	Base	Midbase	Apex
Inner Hair Cells				
vector/host strain				
Syt1-eGFP/Otof	7	20.3 ± 25.1 ¥€	67.4 ± 27.0 †¥	71.1 ± 24.3 ‡€
eGFP/WT	6	20.7 ± 16.3 øh	82.8 ± 21.2 ¤ø	67.5 ± 19.4 h
Syt1-eGFP/WT	4	56.7 ± 24.0	75.9 ± 17.0	62.1 ± 15.5
Outer Hair Cells				
vector/host strain				
Syt1-eGFP/Otof	7	4.57 ± 6.9 î	14.2 ± 14.0 †*	35.1 ± 23.0 ‡î
eGFP/WT	6	9.8 ± 7.7 ?§	36.0 ± 19.3 ¤?*	41.0 ± 20.0 §
Syt1-eGFP/WT	4	27.1 ± 17.0	30.3 ± 24.7	42.9 ± 56.5

î p=.02,

‡ p=.009,

€ p=.006,

¥ p=.003,

† p=.001,

? p=.03,

§ p=.02,

h p=.005,

ø p=.003,

¤ p=.002, by repeated measures ANOVA;

* p=.04, by paired samples t- test